

Impact of ice crystal development on electrical impedance characteristics and mechanical property of green asparagus stems

メタデータ	言語: eng 出版者: 公開日: 2021-01-04 キーワード (Ja): キーワード (En): 作成者: 安藤, 泰雅, 萩原, 昌司, 鍋谷, 浩志, 奥西, 智哉, 岡留, 博司 メールアドレス: 所属:
URL	https://repository.naro.go.jp/records/4964

This work is licensed under a Creative Commons Attribution-NonCommercial-ShareAlike 3.0 International License.



1

2 **Impact of Ice Crystal Development on Electrical Impedance Characteristics and**
3 **Mechanical Property of Green Asparagus Stems**

4

5

6 Yasumasa ANDO ^{a,*}, Shoji HAGIWARA ^b, Hiroshi NABETANI ^{b,c}, Tomoya

7 OKUNISHI ^b, Hiroshi OKADOME ^b

8 ^a Institute of Vegetable and Floriculture Science, NARO, 360 Kusawa, Anou, Tsu, Mie

9 514-2392, Japan.

10 ^b Food Research Institute, NARO, 2-1-12 Kannondai, Tsukuba, Ibaraki 305-8642, Japan.

11 ^c Graduate School of Agricultural and Life Sciences, The University of Tokyo, 1-1-1

12 Yayoi, Bunkyo-ku, Tokyo 113-8657, Japan.

13

14 Corresponding author: Yasumasa Ando, Institute of Vegetable and Floriculture Science,

15 NARO, 360 Kusawa, Anou, Tsu, Mie 514-2392, Japan.

16 E-mail yaando@affrc.go.jp

17 Tel +81-50-3533-4628

18 **Abstract**

19 The effects of ice crystal formation during freezing using three different
20 methods: slow freezing, air blast freezing and liquid nitrogen spray freezing on the cell
21 membrane state and mechanical property of asparagus stem samples were investigated.
22 X-ray computed tomographic analysis revealed coarser ice crystal growth with slow
23 freezing compared to the rapid freezing methods, which were characterized by fine and
24 homogeneous ice crystal growth. However, electrical impedance analysis clarified that
25 the structural damage and functional decline of cell membranes occurred regardless of
26 the freezing method. Further, the elastic property of each frozen sample declined greatly
27 after thawing and showed little improvement with rapid freezing. These results suggest
28 that the reduction in turgor pressure following changes in the cell membrane state,
29 attributable to the formation of ice crystals during freezing, is a major factor in the
30 mechanical property, and this phenomenon is independent of the freezing rate and ice
31 crystal size.

32

33 **Keywords:** Freezing, Ice crystal, X-ray computed tomography, Electrical impedance
34 spectroscopy, Mechanical property, Asparagus stem

35 **Nomenclature**

36

37	C_m	capacitance of cell membrane (F)
38	j	imaginary unit (–)
39	P	constant phase element exponent (–)
40	R	real part of the impedance (Ω)
41	R_i	intracellular fluid resistance (Ω)
42	R_e	extracellular fluid resistance (Ω)
43	T	constant phase element coefficient ($F \cdot s^{(P-1)}$)
44	X	imaginary part of the impedance (Ω)
45	Z	complex impedance (Ω)
46	Z_{CPE}	impedance of constant phase element (Ω)
47	θ	phase angle (rad)
48	ω	angular frequency (rad/s)

49 **1. Introduction**

50

51 Freezing is one of the main methods employed for long-term food preservation,
52 which inhibits microbial, metabolic and enzymatic activities, offering convenience for
53 consumers and superior taste retention and nutritional value compared to other methods.
54 However, changes in the physical and chemical structures resulting from the formation
55 and growth of ice crystals during freezing can lead to the degradation of food quality.
56 The characteristics of ice crystals, e.g., size, shape and distribution, formed during
57 freezing are closely related to the quality of frozen foods. Therefore, many studies have
58 aimed to elucidate the mechanism of ice crystal formation and the characteristics of ice
59 crystals formed in foods (Kiani & Sun, 2011; Chevalier et al., 2000).

60 The formation of ice crystals requires two stages: the generation of ice nuclei,
61 followed by the growth of crystals (Delgado & Sun, 2001). Since the moisture in foods
62 forms fine and homogeneous ice crystals when subjected to the temperature range for
63 crystal growth over a short period, causing less deterioration in quality, (Chevalier et al.,
64 2000; Kono et al., 2017), various rapid freezing methods have been employed in the
65 field of practical frozen food production for quality improvement. Additionally,
66 technology to control ice crystal formation in foods such as ultrasonic freezing, which
67 facilitates ice nucleation (Zheng & Sun, 2006; Bhaskaracharya et al., 2009), pressure
68 shift freezing (Otero & Sanz, 2000; LeBail et al., 2002) and supercooling application
69 (Miyawaki et al., 1992; Kobayashi et al., 2015) to minimize and homogenize ice crystal
70 formation have been reported. In these ongoing studies, the technique to visualize the
71 3D structure of ice crystals by X-ray computed tomography (X-ray CT) proposed by

72 Mousavi et al. (2005) has been expanded for the effective evaluation of ice crystal
73 characteristics. Since then, the technique has been widely applied to understand the
74 growth behavior of ice crystals at sub-zero temperatures in food materials such as
75 soybean curd (Harnkarnsujarit et al., 2016a), polysaccharide gels (Harnkarnsujarit, et al.,
76 2016b), tuna meat (Kobayashi et al., 2015) and potato tissue (Ullah et al., 2014; Zhao &
77 Takhar, 2017).

78 During the freezing of vegetables, depolymerization of the cell wall, rupture of
79 cell membranes and alteration of osmotic pressure triggered by ice crystal formation
80 lead to losses of cell wall rigidity and cellular turgor, resulting in significant
81 modification of the mechanical property after thawing (Li et al., 2018). Several previous
82 studies have associated the changes in mechanical properties with the structural
83 destruction of the cell wall following the formation and expansion of ice crystals during
84 freezing (Paciulli et al., 2015; Van Buggenhout et al., 2006; Fuchigami et al., 1995).
85 However, especially in plant cells with low water permeability, the dehydration stress
86 caused by ice crystal growth in the extracellular region leads to fatal disruption of cell
87 membranes and results in significant texture deterioration (Ando et al., 2012). Although
88 the loss of turgor with cell membrane rupture has been considered to be one of the
89 major factors that affect the elastic property of tissues (Ando et al., 2012; Li et al., 2018),
90 it remains unclear how difference in the freezing rate and characteristics of ice crystals
91 formed contribute to the degree of cell membrane damage and the mechanical property.

92 Electrical impedance spectroscopy (EIS) has been employed as a method to
93 quantitatively evaluate the structural damage of cell membranes of biological tissues

94 (Pliquet, 2010). In EIS, the measured impedance frequency characteristics are generally
95 analyzed using the equivalent circuit model (Zhang et al., 1990; Yamamoto &
96 Yamamoto, 1977). Biological tissues are electrically inhomogeneous cell assemblies;
97 thus, a modified model was developed (Ando et al., 2014) by incorporating a constant
98 phase element (CPE) to the cell model proposed by Hayden et al. (1969). Since the
99 values of intra- and extracellular fluid resistance and cell membrane capacitance in
100 biological tissues can be quantified using the modified model, it has been used to
101 evaluate damage in the cell membranes of vegetables and fruits during heating
102 (Watanabe et al., 2017; Ando et al., 2017; Imaizumi et al., 2015), drying (Ando et al.,
103 2014) and cold storage (Imaizumi et al., 2018; Watanabe et al., 2018).

104 The present study aimed to clarify the influence of the various characteristics of
105 ice crystals formed at different freezing rates on cell membrane damage and mechanical
106 property. The X-ray CT technique was applied to evaluate ice crystal characteristics in
107 asparagus stems, which are commonly consumed as a frozen product throughout the
108 world, and then the relationship between ice crystal characteristics, cell membrane
109 damage as quantified by EIS analysis and the compressive elastic property after
110 freezing-thawing was investigated.

111

112 **2. Materials and methods**

113

114 *2.1 Sample preparation*

115 Stems of green asparagus (*Asparagus officinalis* L.) were obtained from a local

116 market, stored in a refrigerated chamber at 5 °C, and used for the experiments within 3
117 days. The asparagus stem (initial length of 270 mm) was cut into thirds perpendicular to
118 the fiber direction, then the central part was cut into 30 mm length (diameter of 10–12
119 mm), and used as the sample. For the mechanical test only, four samples were cut into
120 10 mm length from one stem and distributed to each test section to minimize individual
121 differences. The samples were blanched in boiling water for 1 min, then immediately
122 cooled in iced water.

123

124 2.2 *Freezing procedure*

125 The blanched samples were frozen by slow (SL) freezing, air blast (AB)
126 freezing or liquid nitrogen spray (LNS) freezing as slow, intermediate and rapid rate of
127 freezing respectively. In the SL freezing, the samples were placed on a polystyrene foam
128 board and frozen in a freezer (SF-3120F3, Nihon Freezer, Tokyo, Japan) at –30 °C. AB
129 freezing was carried out in a freezer (FMF-038F1, Fukushima Industries Corp., Osaka,
130 Japan) equipped with four fans (9GT, Sanyo Denki Co., Ltd., Tokyo, Japan) at a
131 temperature of –40 °C and an air velocity of 2.8 m/s. Samples frozen in a liquid
132 nitrogen spray freezer (EMP-10NS, Ebara Inc., Tokyo, Japan) at a temperature of
133 –60 °C and an air velocity of 1.4 m/s were used as the LNS frozen sample. After
134 freezing, the samples were immediately offered for the measurement process described
135 below. The samples were thawed at room temperature (25 °C) for 2 h, and used for the
136 experiments. The temperature of the central part of the sample during freezing was
137 measured using a T-type thermocouple with a wire diameter of 0.34 mm and retrieved

138 in a data logger (GL220, Graphtec Corp., Kanagawa, Japan) at 1 sec intervals.

139

140 2.3 *X-ray CT evaluation of ice crystals*

141 Ice crystals formed in the samples were visualized by the indirect observation
142 method using X-ray computed tomography (CT), as previously reported (Mousavi et al.,
143 2005; Kobayashi et al., 2015). Prior to evaluation using a micro focus X-ray CT system
144 (SMX-100CT, Shimadzu Corp., Kyoto, Japan), ice crystals in the sample were
145 sublimated in a freeze-dryer (FD-20BU, Nihon Techno Service Co., Ltd., Ibaraki,
146 Japan). The temperature of the dryer was gradually increased for 1 week from $-40\text{ }^{\circ}\text{C}$ to
147 $15\text{ }^{\circ}\text{C}$ at a pressure below 10 Pa. It was assumed that the sublimated ice crystals left
148 pores with minimal deformation and that these pores were of the same size as the ice
149 crystals. Both whole samples and samples cut into quarters in parallel to the fiber
150 direction with a sharp knife were scanned using the X-ray CT system at an X-ray tube
151 voltage of 45 kV and a current of 100 μA ; 1800 transmission images were obtained
152 through a 360 degree rotation. Tomographic images were reconstructed using software
153 (Exfact VR, Nihon Visual Science Inc., Tokyo, Japan). Cross-sectional images with
154 $20.7 \times 20.7\ \mu\text{m}^2$ pixel size of the quartered samples were used for estimation of the size
155 distribution of ice crystals. Three samples from each freezing condition were scanned,
156 and 12 cross-sectional images randomly selected from each sample were used for the
157 analysis. The obtained gray-scale images were binarized, then watershed segmentation
158 was applied for the proper detection of ice crystal areas in reference to the literature
159 (Zhao et al., 2017; Haris et al., 1998). Feret's diameter (i.e., line segment connecting the

160 two perimeter points that are the furthest apart) of the ice crystal area was calculated
161 using software (ImageJ version 1.51j8, W. S. Rasband, U. S. National Institutes of
162 Health, Bethesda, MD, USA).

163

164 2.4 *Electrical impedance spectroscopy (EIS)*

165 Electrical impedance characteristics of the samples before and after
166 freezing-thawing were measured using an impedance analyzer (E4990A, Keysight
167 Technologies, Santa Rosa, CA, USA) equipped with stainless needle electrodes. The
168 electrodes spaced 10 mm apart were inserted from the periphery to the central axis of
169 the sample to a depth of 5 mm, and impedance magnitude $|Z|$ (Ω) and phase difference θ
170 (rad) of the sample were measured at 65 points (logarithmic frequency intervals) over
171 the frequency range of 50 to 5 MHz. Before the measurement, the sample temperature
172 was conditioned to a room temperature of 25 °C to prevent temperature differences
173 from influencing the impedance characteristics.

174 The measured impedance data were analyzed using the equivalent circuit
175 model, as shown in Fig. 1. The model by Hayden et al. (1969) shown in Fig. 1 (a),
176 comprised of cell membrane resistance, C_m , and extra- and intracellular fluid resistances,
177 R_e and R_i , respectively, was proposed as a structural model of a single cell in biological
178 tissues. The model shown in Fig. 1 (b) was modified with a constant phase element,
179 CPE (Zoltowski, 1998), and has been proposed (Ando et al., 2014) as a model of
180 biological tissues, taking into account the time constant distribution of the impedance
181 characteristics being attributed to the non-uniform electrical characteristics of cells in

182 the tissue, which has been proven to be a valid model of biological tissues in many
183 studies (Imaizumi et al., 2015; Watanabe et al., 2017). The impedance of CPE (Z_{CPE}) is
184 represented as:

$$185 \quad Z_{CPE} = \frac{1}{(j\omega)^P T}, \quad (1)$$

186 where ω denotes the angular frequency (rad/s), T denotes the CPE coefficient, and P
187 denotes the CPE exponent ($0 \leq P \leq 1$). The measured impedance data were fitted to the
188 equation of the total impedance of model (b) using complex nonlinear least squares
189 curve fitting (Macdonald, 1992), and each circuit parameter was estimated. The root
190 mean squared error, RMSE, was calculated to evaluate the goodness of fit of the model.

191 Here, the CPE constant T was converted to an apparent capacitance C using the
192 equation below (Ando et al., 2014; Hsu & Mansfeld, 2001):

$$196 \quad C = T^{\frac{1}{P}} (R_e + R_i)^{\frac{1-P}{P}}. \quad (2)$$

193 In this study, the apparent capacitance C , obtained from Eq. (2), was defined as the cell
194 membrane capacitance C_m . The detailed protocol of the analysis has been reported
195 previously (Ando et al., 2017).

197

198 2.5 Mechanical property

199 A universal testing machine (5542, Instron, Norwood, MA, USA) equipped
200 with a 500 N load cell was used for sample testing. The sample was compressed by a
201 cylindrical plunger, 1000 mm² in base area at a speed of 0.5 mm·s⁻¹, from the side of
202 the cylinder shape of the sample until the compressive strain reached 50 % of the initial
203 thickness. The trigger load was set to 0.05 N. The diameter of the sample was measured

204 using a caliper. The slope of the initial linear range (strain < 0.1) in the compressive
205 curve was calculated as an index of the elastic property (Ando et al., 2012; Chiralt et al.,
206 2001; Ando et al., 2016). The test was carried out at a room temperature of 25 °C.

207

208 2.6 *Statistical analysis*

209 Statistical analyses were performed using R software version 3.3.3 (R Core
210 Team). Differences among the means were compared using Tukey's multiple range test
211 with analysis of variance at a significance level of $p < 0.05$.

212

213 **3. Results and discussion**

214

215 3.1 *Freezing rate and ice crystal distribution*

216 Figure 2 shows the changes in sample temperature during freezing. In AB
217 freezing, approximately 12 min was needed to reach -20 °C and about 10 min for LNS
218 freezing, while SL freezing required 50 min. In each freezing condition, plateaus were
219 observed around -0.8 °C, indicating the formation and growth of ice crystals in this
220 temperature region. Figure 3 shows cross-sectional images of whole and quartered
221 samples after freeze-drying obtained by X-ray CT. In the freeze-dried SL sample,
222 relatively large voids were observed in the interior, revealing the formation of coarse ice
223 crystals during freezing. In the freeze-dried AB and LNS samples, although slightly
224 coarse voids can be observed in the surface area, finer voids are distributed in most
225 regions, indicating that ice crystals were minimized in the AB and LNS freezing. The

226 relatively coarse ice crystals were formed in the surface area because they were
227 developed at the point of boundary which is presumed to be structurally weak between
228 the cortical tissue just inside the epidermis and the supporting collenchyma tissue. In
229 addition, as is especially pronounced in the AB and LNS samples, ice crystals tended to
230 expand in the vascular bundles interspersed within the parenchyma tissue those have
231 relatively large spaces for ice crystals to grow without being hindered by cell walls.
232 Histograms of the ice crystal diameter extracted from each quartered sample are shown
233 in Fig. 4. It should be noted that the inherent air spaces in the sample tissue and
234 unavoidable slight shrinkage and deformation during freeze-drying process might have
235 affected the evaluation of the ice crystal size. In the SL frozen sample, the histogram
236 peaks around 150–200 μm and gradually declines to over 1000 μm , indicating wide
237 variation in the diameter of ice crystals formed during freezing. In the samples frozen
238 by AB and LNS, the diameter showed a relatively sharper peak and converges to around
239 500 μm , suggesting that fine, homogenously sized ice crystals were formed compared to
240 those in SL sample. Here, the mean values of the ice crystal size of SL, AB and LNS
241 samples were 428, 337 and 317 μm , and median values of those were 380, 320 and 297
242 μm respectively. In general, the size of ice crystals depends on the rate of freezing.
243 Therefore, it was thought that fine, homogenous ice crystals were formed in AB and
244 LNS samples because ice crystal formation occurred over a shorter time period in these
245 samples, as previously reported (Kono et al., 2017; Kobayashi et al., 2015). The larger
246 size of ice crystals observed in this study compared to tuna (Kobayashi et al., 2015) and
247 mycoprotein (Mousavi et al., 2005) was attributed to the higher moisture content of

248 vegetable tissues (typically greater than 90 %). Although the ice crystal size of the LNS
249 sample was slightly finer than those of AB sample, notable differences was not observed
250 between AB and LNS, suggesting that a large decrease in ice crystal size cannot be
251 expected by excess increases in the freezing rate as reported by the previous study in
252 which the ice crystal diameter declined exponentially with increases in the freezing rate
253 (Kono et al., 2017).

254

255 3.2 *Evaluation of cell membrane damage*

256 Figure 5 shows the impedance characteristics on the complex plane (Cole-Cole
257 plot) of the fresh, blanched and each frozen-thawed samples. The impedance
258 characteristics of the fresh samples displayed as a large arc, while the impedance of the
259 blanched sample and each frozen-thawed samples showed significantly compressed arcs.
260 Generally, the Cole-Cole plot of biological tissues that have a cellular structure is
261 described as a circular arc (Cole, 1932); therefore, the large arc of the impedance
262 characteristics of the fresh sample indicates that the cell membrane structure was
263 normally maintained. Compression of a Cole-Cole plot was reported in the drying of
264 potatoes (Ando et al., 2014), freezing of potatoes (Zhang & Willison, 1992) and heating
265 of spinaches (Watanabe et al., 2016), and the phenomenon was thought to be a result of
266 cell membrane injury. Therefore, the results obtained in this study suggest that cell
267 membranes in the sample tissues were injured during blanching and the
268 freezing-thawing process, and the smaller size of the arcs of the frozen-thawed samples
269 suggests that the freezing treatment caused greater cell membrane damage compared to

270 blanching treatment.

271 In this study, the obtained impedance characteristics were analyzed with the
272 modified Hayden model, shown as model (b) in Fig. 1. Solid lines in Fig. 5 represent
273 approximations given by the model fitted using the complex nonlinear least squares
274 method. Here, only the arc region of the impedance spectra was used for the fitting,
275 since the other region is not related to the cellular structure (Ando et al., 2014). The
276 measured impedance spectra and solid lines were well matched for all samples (the ratio
277 of RMSE to the average of measured impedance value was less than 0.8 %), which
278 confirms that the present model is reasonable for application to the samples.

279 The estimated values of the model parameters: cell membrane capacitance, C_m ,
280 extracellular fluid resistance, R_e , and intracellular resistance, R_i , are shown in Table 1.
281 The value of C_m , which depends on the lipid bilayer structure of the membrane
282 (Ashrafuzzaman & Tuszynski, 2013) of the fresh sample, was the highest, indicating
283 that the structure was substantially maintained. However, in the blanched sample, C_m
284 was reduced to one-quarter or less of that of the fresh sample, suggesting structural
285 damage of cell membranes by heat treatment. The same phenomenon has been reported
286 for spinach (Watanabe et al., 2017) and Japanese radish (Ando et al., 2017), and is
287 presumed to be attributable to thermal denaturation of phospholipids contained in the
288 cell membrane. The C_m values of each frozen-thawed sample were greatly decreased to
289 1.0–1.2 % of the fresh sample, and there was no significant difference between each
290 freezing method. Cell membrane injury of plant tissues during freezing has been
291 reported in many studies, which propose that the formation of ice crystals during

292 freezing is responsible for cell membrane damage (Ando et al., 2012; Delgado &
293 Rubiolo, 2005). Although the results obtained in this study support this viewpoint, the
294 level of cell membrane damage was comparable with all freezing methods despite the
295 difference in the size of ice crystals, which suggests that the phenomenon of cell
296 membrane damage during freezing is independent of ice crystal size.

297 The high values of R_e and the low value of R_i of the fresh sample were due to
298 the low electrolyte concentration of the extracellular fluid and the high electrolyte
299 concentration of the intracellular fluid, indicating that the permselectivity of the cell
300 membrane is functioning normally. In the blanched sample, R_e was decreased and R_i
301 was increased because the difference in the electrolyte concentration between the intra-
302 and extra-cellular fluids could not be maintained due to the decline in cell membrane
303 function. In the frozen-thawed sample, R_e decreased markedly and in contrast to the
304 fresh and blanched samples, R_i had a larger value than R_e . As in the case of C_m , there
305 was no significant difference in R_e and R_i between each freezing method. In the
306 freezing process, the cell interior is rapidly dehydrated concomitant with ice crystal
307 growth in the extracellular region (Palta, 1990), and results in a cell volume decrease
308 due to plasmolysis. Further decreases in the R_e of frozen-thawed samples could be
309 explained by the increase in the amount of extracellular fluid due to the above
310 phenomenon, which resulted in the increase of the electrical flow path and decrease in
311 electrical resistance. Conversely, the increase in R_i value was attributed to limitation of
312 the electrical flow path from the decrease in intracellular volume. These changes in
313 model parameters were also observed in the fresh-frozen samples (not blanched) by

314 each freezing method, and there was no significant difference due to the presence or
315 absence of blanching (data not shown), indicating that freezing-thawing has a greater
316 influence on cell membrane damage than blanching.

317 From the above results, it was shown that the cell membrane was structurally
318 and functionally damaged during the freezing-thawing process, and that this
319 phenomenon was not dependent on ice crystal size. As noted above, intracellular
320 moisture is rapidly dehydrated in response to ice crystal formation and growth during
321 freezing. In addition, during freezing-thawing, cells are subjected to a multitude of
322 stresses including chilling stress, and mechanical and chemical stresses resulting from
323 ice crystal formation (Steponkus, 1984). However, the results obtained suggest that the
324 cell membrane damage resulting from the above causes cannot be prevented by
325 minimizing ice crystal size with a rapid rate of freezing.

326

327 3.3 *Mechanical properties after thawing*

328 Figure 6 shows the representative compressive curve of the blanched and each
329 frozen-thawed samples. In the blanched sample before freezing, the force increased with
330 compression and reached over 30 N, and fracture occurred in the sample around a strain
331 of 0.5. The increase in force was suppressed in the frozen-thawed samples, suggesting a
332 decrease in tissue rigidity, and fracture was not observed in each freezing method.

333 Although the force in the LNS and AB frozen samples seemed to be slightly higher than
334 that of the SL frozen sample, the difference between the freezing methods was quite
335 small and the forces were significantly decreased compared to the blanched sample. The

336 initial slope from the origin to the force at a strain of 0.1 in the force-strain curve is
337 shown in Table 2 as an index of the elastic property of the samples. The values after
338 freezing were greatly decreased to 22–32 % of the blanched sample. In a comparison of
339 each freezing method, the initial slopes of the rapid freezing methods (AB and LNS)
340 were slightly higher than that of SL. However, the ability to improve the change in the
341 mechanical property was limited even by rapid freezing, and the substantial change
342 during freezing-thawing could not be inhibited. Decline in the mechanical property after
343 freezing-thawing of vegetables has been reported previously (Paciulli et al., 2015; Van
344 Buggenhout et al., 2006; Fuchigami et al., 1995), and this phenomenon was considered
345 as the result of the destruction of the tissue structure, e.g., the cell wall, following ice
346 crystal formation. However, although smaller ice crystals were formed by rapid freezing
347 in this study, substantial improvement in the mechanical property was not observed
348 compared to slow freezing, in which coarse ice crystals were obviously formed. As
349 shown by the impedance analysis, the structural damage and functional decline of the
350 cell membrane during freezing-thawing occurred equally among each freezing condition.
351 These changes in the cell membrane state cause the loss of turgor pressure, which has a
352 large impact on the mechanical properties, especially the elastic property of vegetables
353 (Gonzalez, Anthon, & Barrett, 2010; Greve et al., 1994). Therefore, as suggested by
354 Chassagne-Berces et al. (2009) and Ando et al. (2012), it was assumed that a reduction
355 in turgor pressure following changes in the cell membrane state, resulting from ice
356 crystal formation during freezing, is a major factor in the mechanical property. Further,
357 the results obtained indicate that this phenomenon is independent of freezing rate and

358 ice crystal size.

359

360 **4. Conclusions**

361

362 In the present study, the influence of the size of ice crystals formed in
363 asparagus stem tissue on the cell membrane state and mechanical property was
364 investigated. Although finer ice crystals were observed in the rapid freezing methods,
365 the structural damage and functional decline as estimated by electrical impedance
366 analysis were at the same level as those of the slow-frozen sample, in which coarse ice
367 crystals were clearly observed. Also, the elastic property of the samples after thawing
368 was greatly reduced as compared with those before freezing, and improvements by
369 rapid freezing were limited. These results suggest that the decline in the mechanical
370 property is mainly attributed to the structural damage and functional decline of cell
371 membranes following ice crystal formation during freezing, rather than the size of ice
372 crystals. Although it has been believed that the finer ice crystals formed at faster rate of
373 freezing leads to the improvement of quality after thawing, the present study showed
374 that the fine ice crystals do not necessarily bring about texture improvement in
375 vegetable tissue. Therefore, inhibition of changes in the cell membrane state that occur
376 during freezing and maintenance of turgor pressure are important factors that should be
377 addressed in order to further improve the textural quality of frozen vegetables.

378

379 **Acknowledgement**

380

381 This work was supported by JSPS KAKENHI Grant Number JP18K14554.

382

383 **References**

384

385 Ando, H., Kajiwara, K., Oshita, S., & Suzuki, T. (2012). The effect of osmotic
386 dehydrofreezing on the role of the cell membrane in carrot texture softening
387 after freeze-thawing. *Journal of Food Engineering*, *108*, 473–479.

388 Ando, Y., Mizutani, K., & Wakatsuki, N. (2014). Electrical impedance analysis of potato
389 tissues during drying. *Journal of Food Engineering*, *121*, 24–31.

390 Ando, Y., Maeda, Y., Mizutani, K., Wakatsuki, N., Hagiwara, S., & Nabetani, H. (2016).
391 Effect of air-dehydration pretreatment before freezing on the electrical
392 impedance characteristics and texture of carrots. *Journal of Food Engineering*,
393 *169*, 114–121.

394 Ando, Y., Hagiwara, S., & Nabetani, H. (2017). Thermal inactivation kinetics of pectin
395 methylesterase and the impact of thermal treatment on the texture, electrical
396 impedance characteristics and cell wall structure of Japanese radish (*Raphanus*
397 *sativus* L.). *Journal of Food Engineering*, *199*, 9–18.

398 Ashrafuzzaman, M., & Tuszynski, J. A. (2013). Structure of membranes. In *Membrane*
399 *Biophysics* (pp.9–30). Springer-Verlag Berlin Heidelberg.

400 Bhaskaracharya, R. K., Kentish, S., & Ashokkumar, M. (2009). Selected applications of
401 ultrasonics in food processing. *Food Engineering Reviews*, *1*, 31–49.

402 Chassagne-Berces, S., Poirier, C., Devaux, M. F., Fonseca, F., Lahaye, M., Pigorini, G.,
403 Girault, C., Marin, M., & Guillon, F. (2009). Changes in texture, cellular
404 structure and cell wall composition in apple tissue as a result of freezing. *Food*
405 *Research International*, 42, 788–797.

406 Chevalier, D., Le Bail, A., & Ghoul, M. (2000). Freezing and ice crystals formed in a
407 cylindrical food model: part I. Freezing at atmospheric pressure. *Journal of Food*
408 *Engineering*, 46, 277–285.

409 Chiralt, A., Martínez-Navarrete, N., Martínez-Monzó, J., Talens, P., Moraga, G., Ayala,
410 A., & Fito, P. (2001). Changes in mechanical properties throughout osmotic
411 processes: cryoprotectant effect. *Journal of Food Engineering*, 49, 129–135.

412 Cole, K. S. (1932). Electric phase angle of cell membranes. *Journal of General*
413 *Physiology*, 15, 641–649.

414 Delgado, A. E., & Rubiolo, A. C. (2005). Microstructural changes in strawberry after
415 freezing and thawing processes. *LWT-Food Science and Technology*, 38, 135–
416 142.

417 Delgado, A. E., & Sun, D. W. (2001). Heat and mass transfer models for predicting
418 freezing processes—a review. *Journal of Food Engineering*, 47, 157–174.

419 Fuchigami, M., Miyazaki, K., & Hyakumoto, N. (1995). Frozen carrots texture and
420 pectic components as affected by low-temperature-blanching and quick freezing.
421 *Journal of Food Science*, 60, 132–136.

422 Gonzalez, M. E., Anthon, G. E., & Barrett, D. M. (2010). Onion cells after high pressure
423 and thermal processing: comparison of membrane integrity changes using

424 different analytical methods and impact on tissue texture. *Journal of food*
425 *science*, 75, E426–E432.

426 Greve, L. C., Shackel, K. A., Ahmadi, H., McArdle, R. N., Gohlke, J. R., & Labavitch, J.
427 M. (1994). Impact of heating on carrot firmness: contribution of cellular turgor.
428 *Journal of Agricultural and Food Chemistry*, 42, 2896–2899.

429 Haris, K., Efstratiadis, S. N., Maglaveras, N., & Katsaggelos, A. K. (1998). Hybrid
430 image segmentation using watersheds and fast region merging. *IEEE*
431 *Transactions on Image Processing*, 7, 1684–1699.

432 Harnkarnsujarit, N., Kawai, K., Watanabe, M., & Suzuki, T. (2016a). Effects of freezing
433 on microstructure and rehydration properties of freeze-dried soybean curd.
434 *Journal of Food Engineering*, 184, 10–20.

435 Harnkarnsujarit, N., Kawai, K., & Suzuki, T. (2016b). Impacts of freezing and
436 molecular size on structure, mechanical properties and recrystallization of
437 freeze-thawed polysaccharide gels. *LWT-Food Science and Technology*, 68,
438 190–201.

439 Hayden, R. I., Moyse, C. A., Calder, F. W., Crawford, D. P., & Fensom, D. S. (1969).
440 Electrical impedance studies on potato and alfalfa tissue. *Journal of*
441 *Experimental Botany*, 20, 177–199.

442 Hsu, C. H., & Mansfeld, F. (2001). Technical note: Concerning the conversion of the
443 constant phase element parameter Y-0 into a capacitance. *Corrosion*, 57,
444 747–748.

445 Imaizumi, T., Tanaka, F., Hamanaka, D., Sato, Y., & Uchino, T. (2015). Effects of hot

446 water treatment on electrical properties, cell membrane structure and texture of
447 potato tubers. *Journal of Food Engineering*, 162, 56–62.

448 Imaizumi, T., Yamauchi, M., Sekiya, M., Shimonishi, Y., Tanaka, F. (2018). Responses
449 of components and tissue conditions in persimmon and cucumber to postharvest
450 UV-C irradiation. *Postharvest Biology and Technology*, 145, 33–40.

451 Kiani, H., & Sun, D. W. (2011). Water crystallization and its importance to freezing of
452 foods: A review. *Trends in Food Science & Technology*, 22, 407–426.

453 Kobayashi, R., Kimizuka, N., Watanabe, M., & Suzuki, T. (2015). The effect of
454 supercooling on ice structure in tuna meat observed by using X-ray computed
455 tomography. *International Journal of Refrigeration*, 60, 270–277.

456 Kono, S., Kon, M., Araki, T., & Sagara, Y. (2017). Effects of relationships among
457 freezing rate, ice crystal size and color on surface color of frozen salmon fillet.
458 *Journal of Food Engineering*, 214, 158–165.

459 LeBail, A., Chevalier, D., Mussa, D. M., & Ghoul, M. (2002). High pressure freezing
460 and thawing of foods: a review. *International Journal of Refrigeration*, 25, 504–
461 513.

462 Li, D., Zhu, Z., & Sun, D. W. (2018). Effects of freezing on cell structure of fresh
463 cellular food materials: A review. *Trends in Food Science & Technology*, 75, 46–
464 55.

465 Macdonald, J. R. (1992). Impedance spectroscopy. *Annals of Biomedical Engineering*,
466 20, 289–305.

467 Miyawaki, O., Abe, T., & Yano, T. (1992). Freezing and ice structure formed in protein

468 gels. *Bioscience, Biotechnology, and Biochemistry*, 56, 953–957.

469 Mousavi, R., Miri, T., Cox, P. W., & Fryer, P. J. (2005). A novel technique for ice crystal
470 visualization in frozen solids using X-ray micro-computed tomography. *Journal*
471 *of Food Science*, 70, E437–E442.

472 Otero, L., & Sanz, P. D. (2000). High-pressure shift freezing. Part 1. Amount of ice
473 instantaneously formed in the process. *Biotechnology Progress*, 16, 1030–1036.

474 Paciulli, M., Ganino, T., Pellegrini, N., Rinaldi, M., Zaupa, M., Fabbri, A., & Chiavaro,
475 E. (2015). Impact of the industrial freezing process on selected vegetables—part
476 I. Structure, texture and antioxidant capacity. *Food Research International*, 74,
477 329–337.

478 Palta, J. P. (1990). Stress interactions at the cellular and membrane levels. *Hortscience*,
479 25, 1377–1381.

480 Pliquett, U. (2010). Bioimpedance: A review for food processing. *Food Engineering*
481 *Reviews*, 2, 74–94.

482 Steponkus, P. L. (1984). Role of the plasma membrane in freezing injury and cold
483 acclimation. *Annual Review of Plant Biology*, 35, 543–584.

484 Ullah, J., Takhar, P. S., & Sablani, S. S. (2014). Effect of temperature fluctuations on
485 ice-crystal growth in frozen potatoes during storage. *LWT-Food Science and*
486 *Technology*, 59, 1186–1190.

487 Van Buggenhout, S., Lille, M., Messagie, I., Van Loey, A., Autio, K., & Hendrickx, M.
488 (2006). Impact of pretreatment and freezing conditions on the microstructure of
489 frozen carrots: Quantification and relation to texture loss. *European Food*

490 *Research and Technology*, 222, 543–553.

491 Watanabe, T., Ando, Y., Orikasa, T., Shiina, T., & Kohyama, K. (2017). Effect of short
492 time heating on the mechanical fracture and electrical impedance properties of
493 spinach (*Spinacia oleracea* L.). *Journal of Food Engineering*, 194, 9–14.

494 Watanabe, T., Nakamura, N., Ando, Y., Kaneta, T., Kitazawa, H. & Shiina, T. (2018).
495 Application and simplification of cell-based equivalent circuit model analysis of
496 electrical impedance for assessment of drop shock bruising in Japanese pear.
497 *Food and Bioprocess Technology*, 11, 2125–2129.

498 Watanabe, T., Orikasa, T., Shono, H., Koide, S., Ando, Y., Shiina, T., & Tagawa, A.
499 (2016). The influence of inhibit avoid water defect responses by heat
500 pretreatment on hot air drying rate of spinach. *Journal of Food Engineering*, 168,
501 113–118.

502 Yamamoto, T., Yamamoto, Y., 1977. Analysis for the change of skin impedance.
503 *Medical & Biological Engineering & Computing*, 15, 219–227.

504 Zhang, M. I. N., Stout, D. G., & Willison, J. H. M. (1990). Electrical impedance
505 analysis in plant tissues: Symplasmic resistance and membrane capacitance in
506 the Hayden model. *Journal of Experimental Botany*, 41, 371–380.

507 Zhang, M. I. N., & Willison, J. H. M. (1992). Electrical impedance analysis in plant
508 tissues: *in vivo* detection of freezing injury. *Canadian journal of botany*, 70,
509 2254–2258.

510 Zhao, Y., & Takhar, P. S. (2017). Micro X-ray computed tomography and image analysis
511 of frozen potatoes subjected to freeze-thaw cycles. *LWT-Food Science and*

- 512 *Technology*, 79, 278–286.
- 513 Zheng, L., & Sun, D. W. (2006). Innovative applications of power ultrasound during
514 food freezing processes—a review. *Trends in Food Science & Technology*, 17,
515 16–23.
- 516 Zoltowski, P. (1998). On the electrical capacitance of interfaces exhibiting constant
517 phase element behaviour. *Journal of Electroanalytical Chemistry*, 443, 149–154.

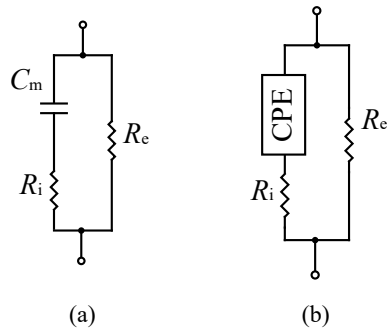


Fig. 1 Equivalent circuit models of biological tissues.
 (a) Hayden model, (b) modified Hayden model. C_m : capacitance of cell membrane,
 R_i : intracellular fluid resistance, R_e : extracellular fluid resistance, CPE: constant phase element.

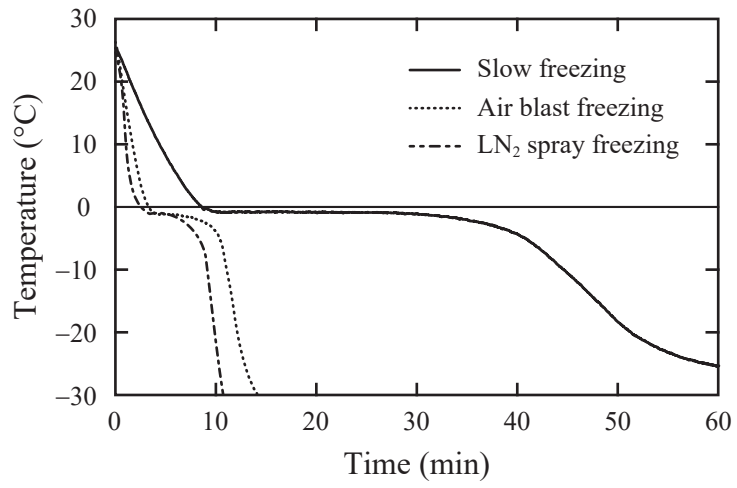


Fig. 2 Changes in the temperature of central part of asparagus samples during freezing.

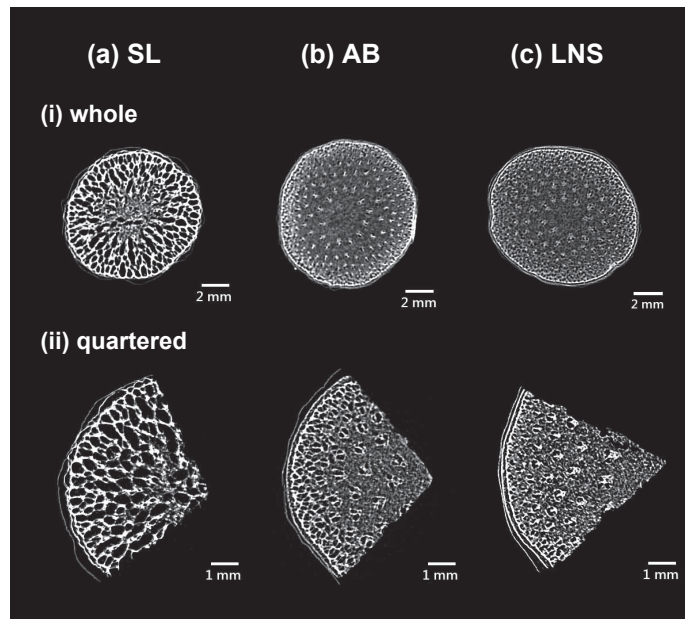


Fig. 3 Representative reconstructed cross-sectional images of whole (i) and quartered (ii) frozen asparagus samples. (a) SL: slow freezing, (b) AB: air blast freezing, (c) LNS: liquid nitrogen spray freezing. Higher brightness part represents higher density part.

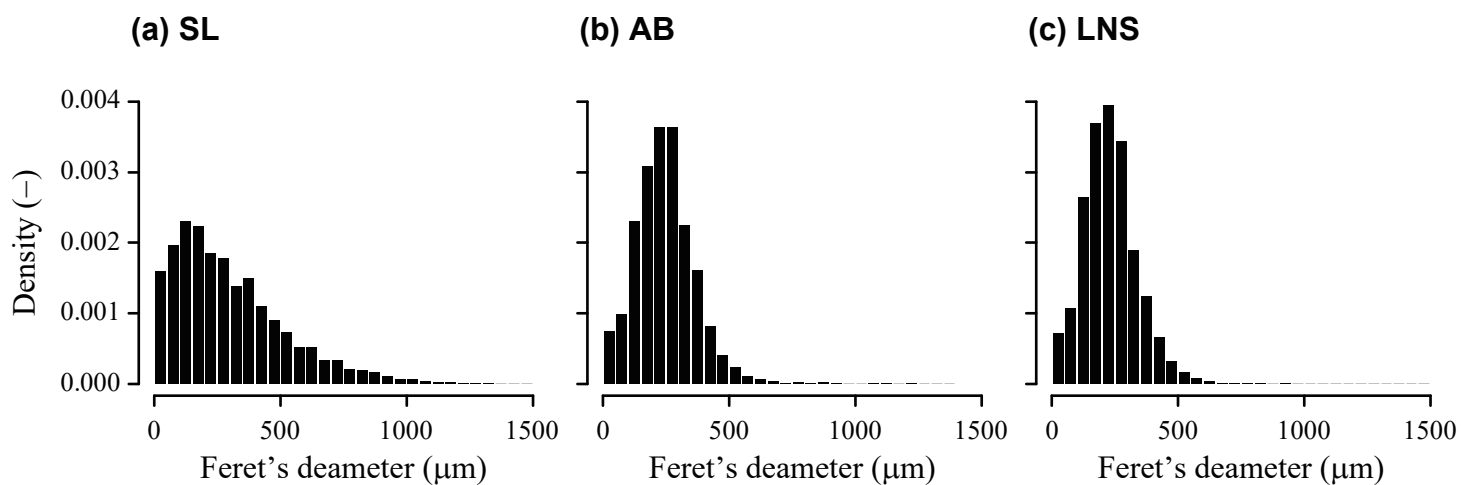


Fig. 4 Ice crystal diameter distribution of frozen asparagus samples. Class interval width of the histograms is 50 μm. (a) SL: slow freezing, (b) AB: air blast freezing, (c) LNS: liquid nitrogen spray freezing. Feret's diameter: line segment connecting the two perimeter points that are the furthest apart.

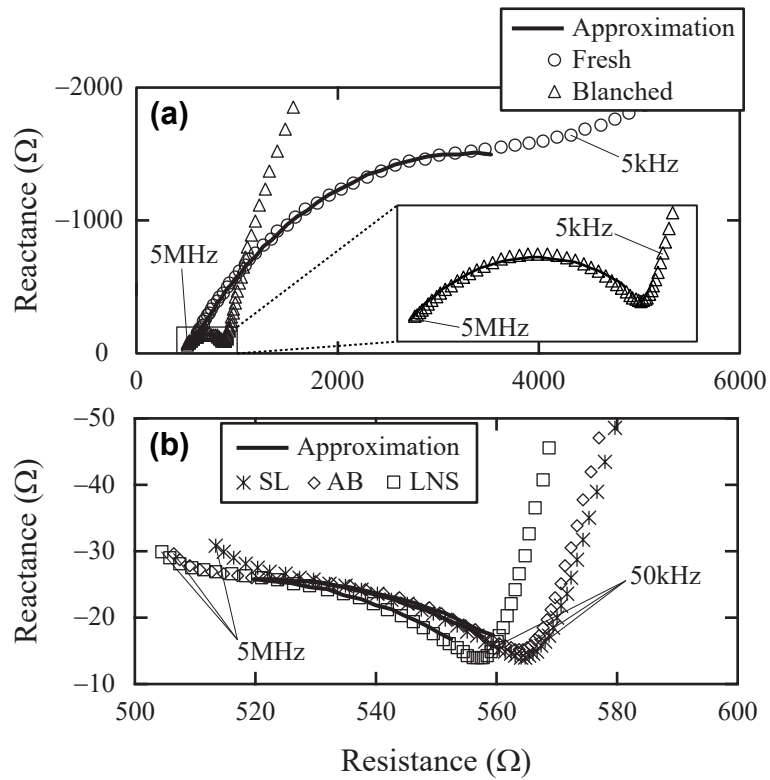


Fig. 5. Representative Cole-Cole plots for the fresh, blanched (a) and frozen-thawed (b) samples. SL: slow freezing, AB: air blast freezing, LNS: liquid nitrogen spray freezing. Solid lines represent approximations given by the modified Hayden model in Fig. 1b.

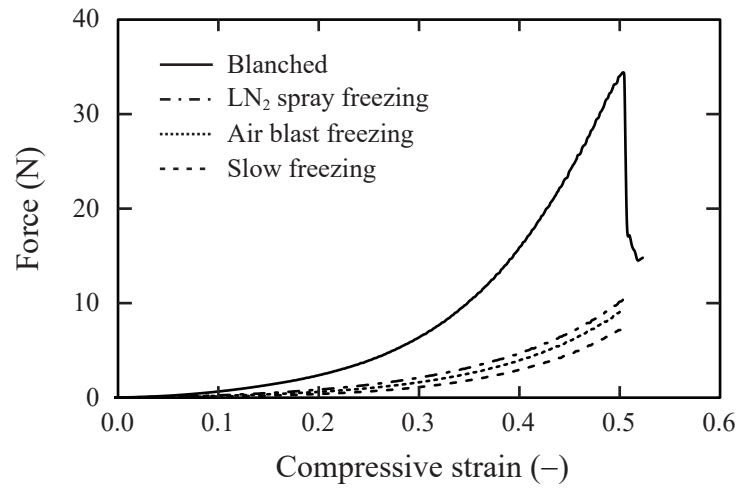


Fig. 6. Representative compressive curves of the blended and frozen-thawed samples.

Figure captions

Fig. 1. Equivalent circuit models of biological tissues. (a) Hayden model, (b) modified Hayden model. C_m : capacitance of cell membrane, R_i : intracellular fluid resistance, R_e : extracellular fluid resistance, CPE: constant phase element.

Fig. 2. Changes in the temperature of central part of asparagus samples during freezing.

Fig. 3. Representative reconstructed cross-sectional images of whole (i) and quartered (ii) frozen asparagus samples. (a) SL: slow freezing, (b) AB: air blast freezing, (c) LNS: liquid nitrogen spray freezing. Higher brightness part represents higher density part.

Fig. 4. Ice crystal size distribution of frozen asparagus samples. Class interval width of the histograms is 50 μm . (a) SL: slow freezing, (b) AB: air blast freezing, (c) LNS: liquid nitrogen spray freezing. Feret's diameter: line segment connecting the two perimeter points that are the furthest apart.

Fig. 5. Representative Cole-Cole plots for the fresh, blanched (a) and frozen-thawed (b) samples. SL: slow freezing, AB: air blast freezing, LNS: liquid nitrogen spray freezing. Solid lines represent approximations given by the modified Hayden model in Fig. 1b.

Fig. 6. Representative compressive curves of the blanched and frozen-thawed samples.

Table 1 Equivalent circuit parameters obtained from the model fitting.

Condition	C_m (pF)	R_e (Ω)	R_i (Ω)	RMSE (Ω)
Fresh	1550 ^a \pm 219	5460 ^a \pm 498	540 ^a \pm 24.4	9.7–31.9
Blanched	355 ^b \pm 35.6	970 ^b \pm 80.9	880 ^b \pm 57.4	3.3–6.0
Blanched and frozen-thawed				
Slow freezing	18.6 ^c \pm 7.4	587 ^c \pm 35.1	2190 ^c \pm 316	0.39–0.78
Air blast freezing	16.2 ^c \pm 9.6	585 ^c \pm 42.2	2140 ^c \pm 336	0.52–0.75
Liquid nitrogen spray freezing	18.4 ^c \pm 9.6	581 ^c \pm 52.5	2250 ^c \pm 142	0.36–0.74

C_m : capacitance of cell membrane, R_e : resistance of extracellular fluid, R_i : resistance of intracellular fluid,

RMSE: root mean squared error. The data are mean values of 11–12 replicates (\pm standard deviation).

Different superscripts denote significant differences ($p < 0.05$).

Table 2 Elastic parameter of the samples determined using the compressive test.

Condition	Initial slope (N)
Blanched	6.2 ^a ± 1.2
Blanched and frozen-thawed	
Slow freezing	1.4 ^c ± 0.2
Air blast freezing	1.8 ^b ± 0.3
Liquid nitrogen spray freezing	2.0 ^b ± 0.4

Initial slope: slope from the origin to the force at strain of 0.1 in the force-strain curve. The data are mean values of 52 replicates (± standard deviation).

Different superscripts denote significant differences ($p < 0.05$).

Highlights

- ▶ Ice crystals formed in asparagus stems during freezing were evaluated by X-ray CT.
- ▶ Fine, homogenous ice crystals were observed with the rapid freezing methods.
- ▶ Structural damage and functional loss of cell membranes occurred with each freezing.
- ▶ The decline in elasticity was slightly improved by rapid freezing methods.
- ▶ The change in cell membrane state is a main factor in texture loss with freezing.